Characterisation of thin films of the organic infra-red emitters Yb- and Er-tris(8-hydroxyquinoline) by X-ray photoemission spectroscopy

ARTICLE *in* SYNTHETIC METALS · SEPTEMBER 2003

Impact Factor: 2.25 · DOI: 10.1016/S0379-6779(03)00106-1

ELSEVIER

Synthetic Metals 139 (2003) 207–213

SYNTHETIC METALS

www.elsevier.com/locate/synmet

Characterisation of thin films of the organic infra-red emitters Yb- and Er-tris(8-hydroxyquinoline) by X-ray photoemission spectroscopy

R.I.R. Blyth [a,*], J. Thompson [a], Y. Zou [b], R. Fink [b,1], E. Umbach [b], G. Gigli [a], R. Cingolani [a]

[a] *Dipartimento di Ingegneria dell'Innovazione, National Nanotechnology Laboratory of INFM, Universita' di Lecce, Via Arnesano, 73100 Lecce, Italy*

[b] *Experimentelle Physik II, Universität Würzburg, Am Hubland, D-97074 Würzburg, Germany*

Received 25 November 2002; received in revised form 17 January 2003; accepted 4 February 2003

Abstract

Thin films of the rare earth tris(8-hydroxyquinolines) YbQ_3 and ErQ_3 were evaporated in ultra-high vacuum, and studied by X-ray photoelectron spectroscopy (XPS). Evaporation was monitored by mass spectroscopy of the major cracking products, which have masses >200 a.m.u. and show further splitting due to wide isotope distributions. C and N 1s XPS data are very similar to those of aluminium tris(8-hydroxyquinolines), implying very similar ligand behaviour, while the O 1s binding energy was significantly higher, indicating a more ionic metal–oxygen bond. YbQ_3 was found to be completely trivalent, with no indication of the mixed valence behaviour observed in other Yb compounds.

Keywords: Mass spectroscopy; Photoemission; Rare earth compounds; Infra-red emitters

1. Introduction

Since the observation of high brightness luminescence from organic molecules [1,2], these materials have attracted ever increasing interest. While there exists a large number of organic molecules, both polymers and oligomers, which emit visible light, there are relatively few which emit in the infra-red in the solid state. The rare earth tris(8-hydroxyquinolines) YbQ_3 [3] and ErQ_3 [4,5], which emit light at 980 nm and 1.5 μm, respectively, are two of the most promising of these materials, as these infra-red emissions represent two of the wavelengths most commonly used for infra-red-based communications technology. As can be seen in Fig. 1, the molecular structure of these materials is analogous to that of the well known organic visible light emitter aluminium tris(8-hydroxyquinoline), AlQ_3, whose full three-dimensional structure can be seen in [6]. While Fig. 1 implies that the physical properties of the rare earth hydroxyquinolines, REQ_3s, would be very similar to those of AlQ_3, the different sizes of the Al and rare earth ions suggests that there may well be significant differences. UV-Vis absorption spectra [4] and IR spectra [7] are largely indistinguishable from those of AlQ_3, but these are dominated by intra-ligand transitions and, therefore, offer little insight into the metal–ligand bond, which is where the REQ_3s would be expected to differ from AlQ_3. X-ray photoemission spectroscopy (XPS), gives more element-specific data, allowing a more direct insight into the metal–ligand bonding. In this paper, we report a study of the deposition of thin films of YbQ_3 and ErQ_3 by mass spectroscopy and XPS, and present a comparison of their XPS core level spectra with those of AlQ_3.

2. Experimental

YbQ_3 and ErQ_3 were synthesised as described in [3]. The experiments were performed in a two-chamber ultra-high vacuum system with a base pressure $<10^{-9}$ mbar. The substrate used was a silver(1 0 0) single crystal, cleaned by repeated cycles of argon ion sputtering and annealing. XPS spectra, at room temperature, were taken using a

* Corresponding author. Tel.: +39-832-320-340; fax: +39-832-326-351.
E-mail address: rob.blyth@unile.it (R.I.R. Blyth).
[1] Present address: Universität Erlangen, Physikalische Chemie II, Egerlandstrasse 3, D-91058 Erlangen, Germany.

0379-6779/$ – see front matter © 2003 Elsevier Science B.V. All rights reserved.
doi:10.1016/S0379-6779(03)00106-1

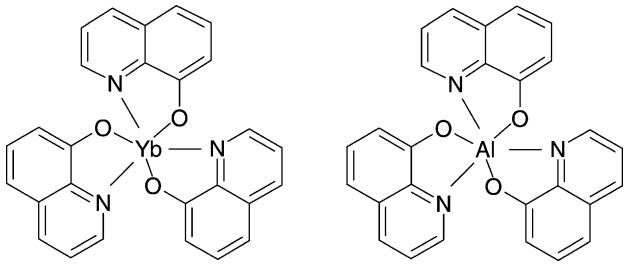

Fig. 1. Schematic diagram of the molecular structures of YbQ_3 and AlQ_3. The true three-dimensional structures show distorted octahedral coordination [6], i.e. the molecules are non-planar.

re-calibrated (absolute accuracy <0.1 eV) Vacuum Generators CLAM 2 analyser, and unmonochromated Mg Kα radiation ($h\nu$ = 1253.6 eV) with an overall resolution of 0.8 eV. The materials were evaporated from a Knudsen cell, mounted in a preparation chamber, in direct line-of-sight with a Balzers QMA400 quadropole mass spectrometer, able to detect masses in excess of 2000 a.m.u.

3. Results

3.1. Mass spectroscopy

The mass spectrum of YbQ_3 during evaporation is shown in Fig. 2. The cracking pattern shows, apart from the parent mass, i.e. REQ_3, major fragments corresponding to the loss of one and two of the quinoline ligands, respectively, REQ_2 and REQ_1, and fragments due to the cracking of the quinoline ligand, Q (90, 117 and 144 a.m.u.). Due to the presence of unreacted quinoline in the source material, and its persistence in the vacuum system, there was always a finite signal corresponding to the quinoline mass in the mass spectrum, even at temperatures well below the evaporation temperatures of the REQ_3 materials. For this reason, the Q signal cannot be used to monitor the evaporation of the REQ materials, even though Q is the major cracking product of REQ_3. Note that of all the possible REQ_3 materials, only the REQ_1 fragment of ScQ_3, with a mass of 188 a.m.u. can be detected by the type of mass spectrometer conventionally used in UHV systems, i.e. one which can not detect masses higher than 200 a.m.u.

Table 1
Isotope distributions [8] and corresponding REQ_3, REQ_2 and REQ_1 fragment masses for YbQ_3 and ErQ_3

Isotope	Percentage occurrence	YbQ_1 mass	YbQ_2 mass	YbQ_3 mass
^{170}Yb	3.0	314	458	602
^{171}Yb	14.3	315	459	603
^{172}Yb	21.8	316	460	604
^{173}Yb	16.1	317	461	605
^{174}Yb	31.8	318	462	606
^{176}Yb	12.8	320	464	608
		ErQ_1 mass	ErQ_2 mass	ErQ_3 mass
^{166}Er	33.6	310	454	598
^{167}Er	22.9	311	455	599
^{168}Er	26.8	312	456	600
^{170}Er	14.9	314	458	602

The parent mass signal of YbQ_3 and ErQ_3, and those of the REQ_2 and REQ_1 fragments showed further splitting, as shown for the REQ_2 fragments in Fig. 3. These splittings do not result from further cracking, but correspond to the isotopic distribution of the rare earths [8], as shown in Table 1.

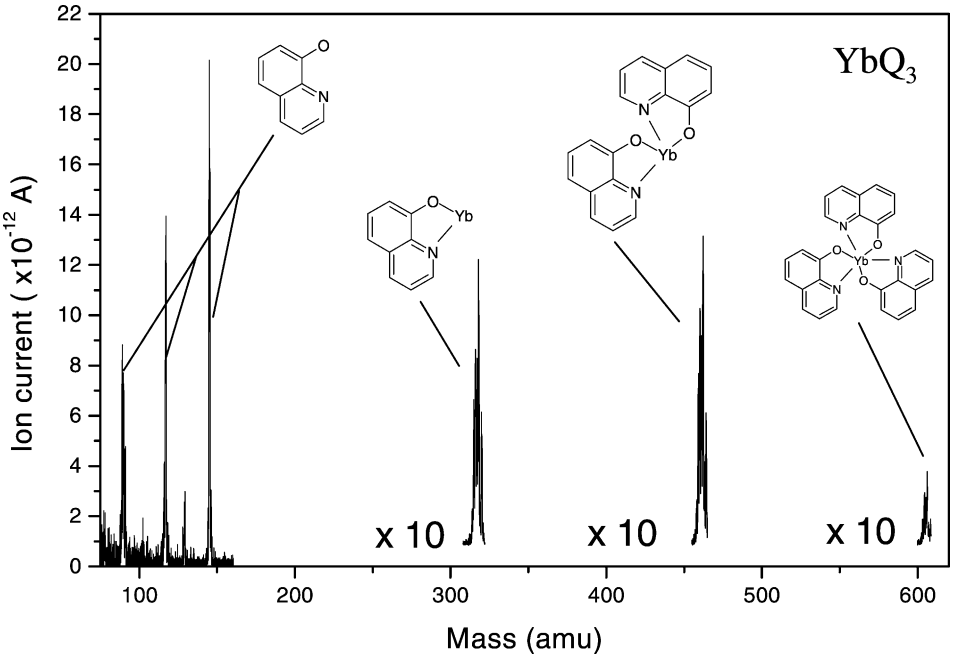

Fig. 2. Mass spectrum of YbQ_3 recorded during evaporation.

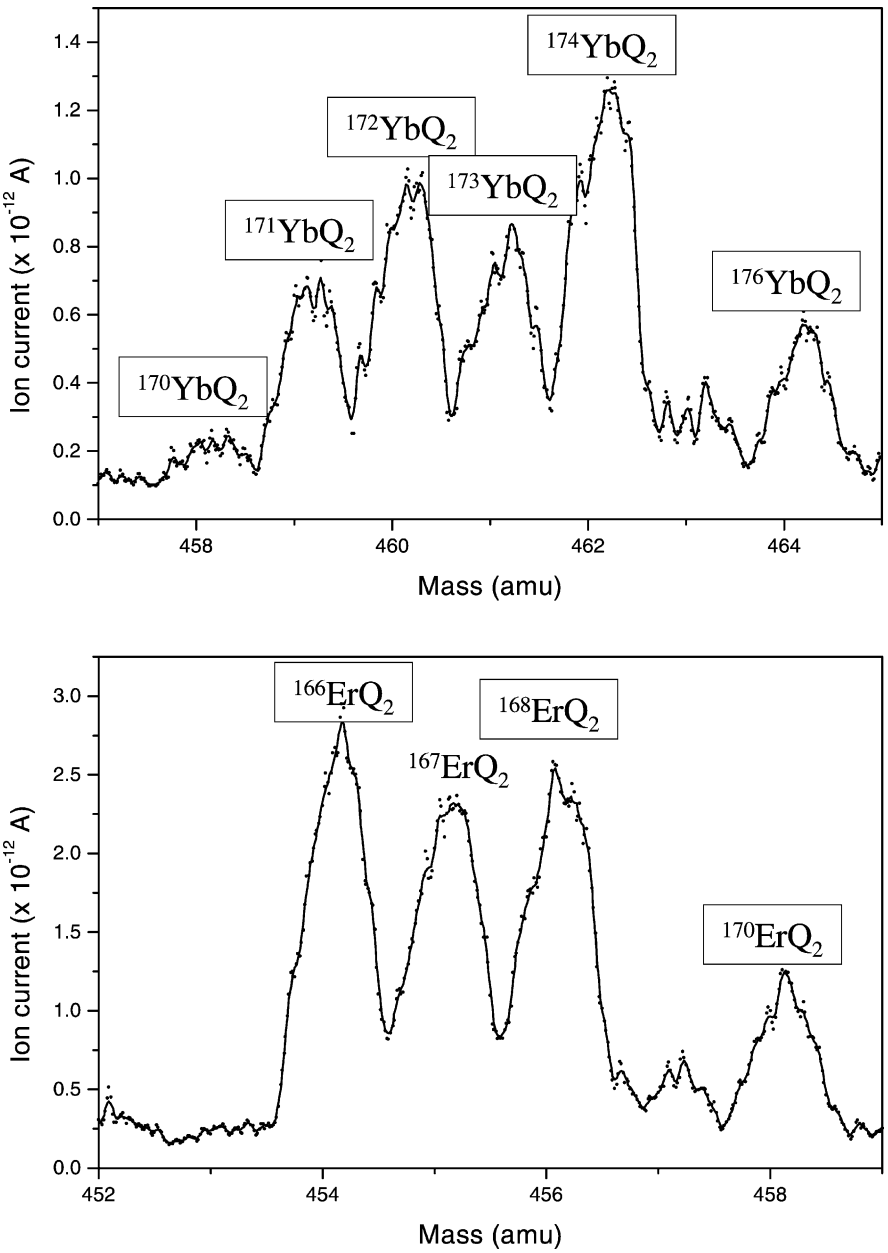

Fig. 3. Mass spectra of the REQ_2 fragments of YbQ_3 and ErQ_3, showing the distribution of rare earth isotopes, recorded during evaporation.

Many of the rare earths have such wide isotope distributions, although there are exceptions, e.g. Tb and Ho. To monitor the evaporation as a function of the Knudsen cell oven temperature, the mass spectrometer was set to record the signal from the most abundant isotope for each of the REQ fragments, as shown in Fig. 4, for ErQ_3. Due to the relative sensitivity of the mass spectrometer, the lighter cracking products appear at lower temperatures than the parent mass. The evaporation temperature for the (slightly heavier) YbQ_3 was slightly higher than for ErQ_3, with the REQ_1 fragment first appearing at 515 K compared to 502 K for ErQ_3. Given the presence of Q fragments in the mass spectrum below the evaporation temperature, degassing was performed for ∼12 h at ∼450 K in order to ensure stochiometric films. The degassing products were largely water and quinoline, the latter, as already stated, being very persistent in the vacuum chamber.

3.2. XPS

Although there is only one RE atom per molecule, compared to 27 carbon atoms and three each of oxygen and nitrogen, the relatively high photoemission cross-sections [9] of, in particular, the RE 4d and 4f levels at this photon energy, ensures that the RE peaks are clearly visible even in a broad scan, as shown for YbQ_3 in Fig. 5. Note that the substrate 3d levels are also visible in Fig. 5. Assuming a homogenous film (which could not be checked, but appears likely for a

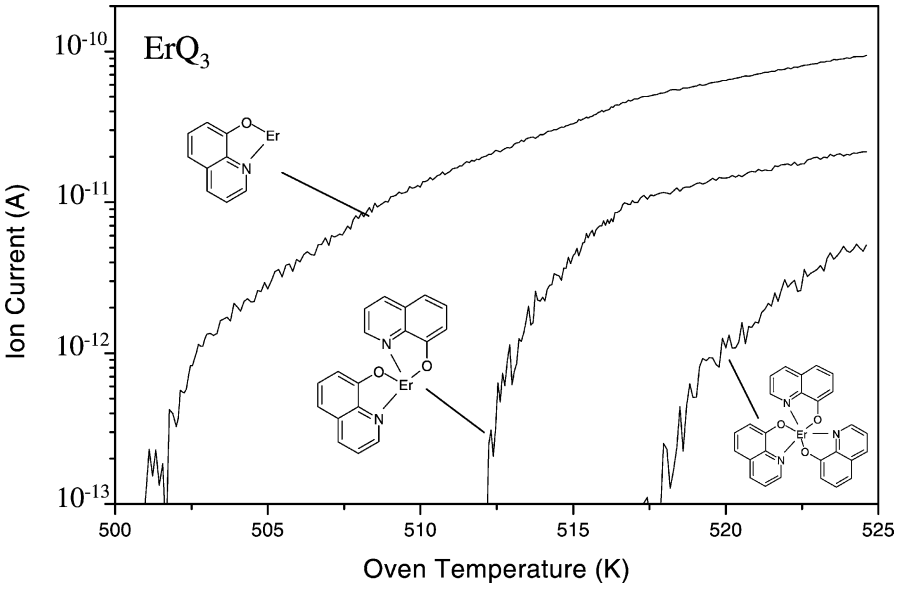

Fig. 4. Evolution of the mass spectrometer signal of the three principal fragments of ErQ_3 as the evaporator Knudsen cell is heated.

material that usually forms amorphous films), this allows an estimate of the film thickness, d, using the expression

$$\frac{I}{I_o} = \exp\left(\frac{-d}{\lambda\cos\theta}\right)$$

where I/I_o is the ratio of the intensities of the substrate 3d peak before and after film deposition, λ the attenuation length of electrons in the organic film, and θ the electron emission angle with respect to the surface normal. For the experimental geometry used, θ is 45°, while for λ we use a value of ∼2 nm, being approximately the attenuation length of electrons with a kinetic energy of ∼1000 eV in organics [10]. The film thickness thus estimated is ∼10 nm, sufficient for the photoemission spectra to be characteristic of the "bulk" material, while thin enough to allow the substrate 3d levels to be monitored as a binding energy reference. No evidence of charging was seen, even in thicker films whose spectra did not show visible 3d peaks.

The O 1s spectra shown in Fig. 6 show no features indicative of impurities. REQ_1 or REQ_2 fragments would have C–O dangling bonds, giving rise to peaks a binding energies ∼1 eV [11] higher than the intrinsic Q_3 peak. This can be seen in the AlQ_3 spectra of Kwon et al. [11], which were taken using a neutralising electron beam, which would be expected to cause some cracking. Unreacted quinoline would have C–O–H bonds, with even higher O 1s binding energies

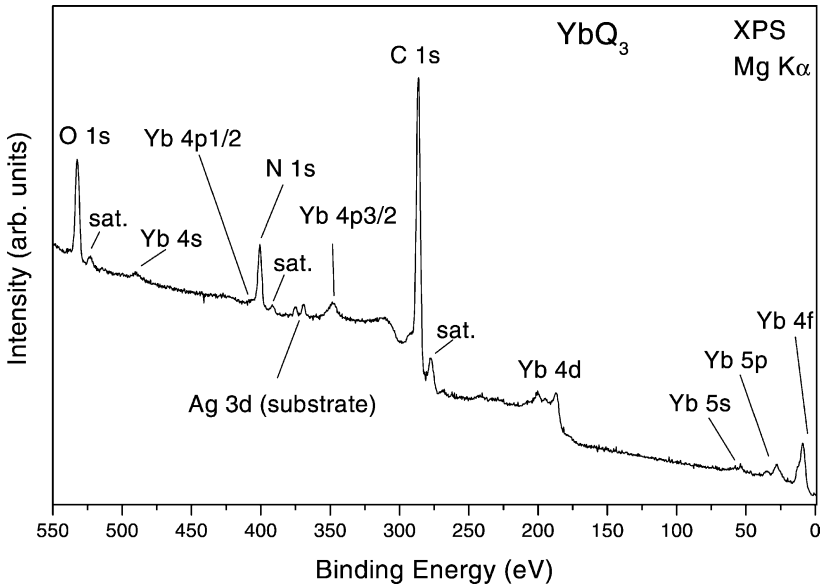

Fig. 5. Broad scan XPS spectrum, $h\nu = 1253.6$ eV, of a thin film (10 nm) of YbQ_3 on Ag(1 0 0).

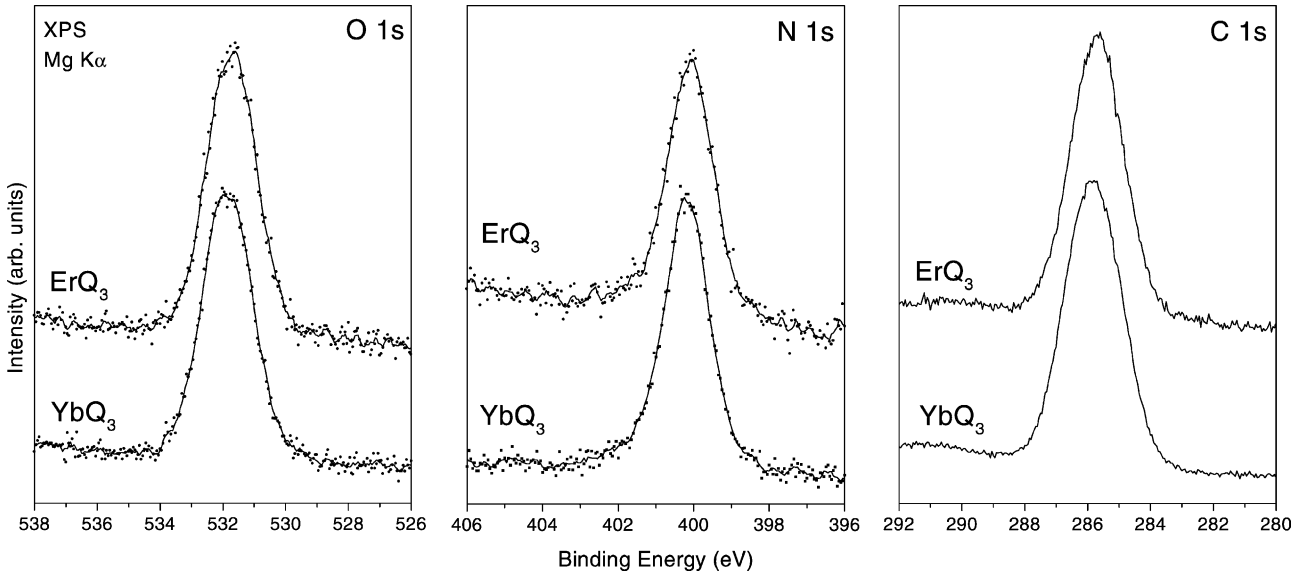

Fig. 6. Oxygen, nitrogen and carbon 1s core level XPS spectra, $h\nu = 1253.6$ eV, of thin films of YbQ_3 and ErQ_3 on Ag(1 0 0).

[12]. Neither cracked nor unreacted material is evident in the O 1s spectra of Fig. 6, within the limits of the resolution. This suggests that the cracking evident in the mass spectra occurs in the mass spectrometer, and not during evaporation, and that the persistent Q presence does not significantly affect film composition. The carbon 1s peak is rather broad, with a width of 1.8 eV, as there are four inequivalent carbon sites, as shown in Fig. 1. This is also observed for XPS spectra of AlQ_3 [13], which of course has the same four sites. The four components are not resolved in Fig. 6, which is not surprising as the resolution is not particularly high, however, they are also not resolved in the (presumably) higher resolution AlQ_3 data of [13], suggesting that this is due rather to solid state broadening. The binding energies of the spectra in Fig. 6 are compared with those of AlQ_3 in Table 2. The binding energies of the C and N 1s peaks in the REQs are essentially identical with those of AlQ_3. Since there are no direct metal–C bonds, the C 1s binding energy is largely a function of the ligand only, and provides further confirmation that the form of the ligand in these materials is essentially the same. Calculations [6,14] show that in the ionic metal–ligand bond of AlQ_3, the transferred electrons are localised mainly on the oxygen site. Therefore, the nitrogen plays little part in the metal–ligand bond and, so it is not unexpected that the N 1s binding energy does not change in going from AlQ_3 to REQ_3. This cannot be said for the O 1s binding energy, which can be seen to be significantly higher in REQ_3 compared to AlQ_3. The ionic radius of Al(III) is 53 pm, whereas, for Er(III) and Yb(III) it is 103 and 117 pm, respectively [8], due to the improved screening induced by the extra intervening atomic shells for the heavier elements, which in turn allows a more ionic bond to be formed with the neighbouring oxygen. The increased binding energy compared to AlQ_3 is consistent with a greater stability and higher ionicity of the metal–oxygen bond.

Table 2
Comparison of the binding energies of the C, O and N 1s peaks of YbQ_3, ErQ_3 and AlQ_3

Peak	YbQ_3	ErQ_3	AlQ_3 [13]
C 1s	285.8	285.7	285.6
N 1s	400.2	400.1	400.2
O 1s	531.9	531.7	531.1

The 4d spectra of the REs are shown in Fig. 7. In principle, information on the nature of the RE–O bond could be obtained by a comparison of the binding energies of the 4d levels with those of other RE compounds. The literature contains very few systematic studies of rare earth compounds with, apart from the sesquioxides, only systematic studies

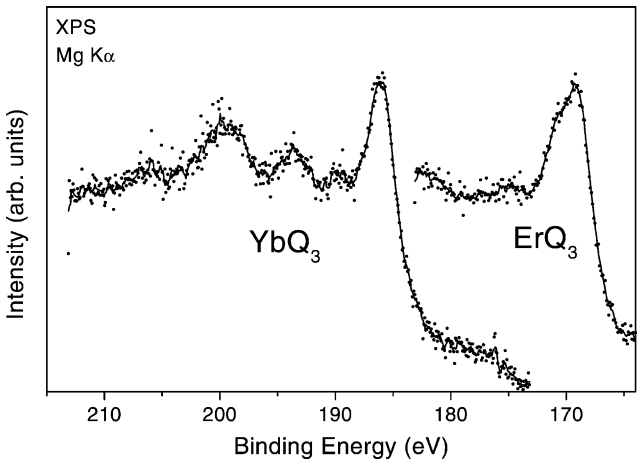

Fig. 7. Rare earth 4d XPS spectra, $h\nu = 1253.6$ eV, of thin films of YbQ_3 and ErQ_3 on Ag(1 0 0).

Table 3
Comparison of the rare earth 4d binding energies in YbQ and ErQ_3 with those of the elements in their metallic state, and those of other rare earth compounds

Peak	YbQ_3	Yb metal[a] [16]	Yb_2O_3 [15]	$Yb_2(C_2O_4)_3$ [15]	$Yb_2(SO_4)_3$ [15]
Yb 4d	186.1	181.4	185.0	187.1	187.1
C 1s	285.8	–	–	289.8	–
O 1s	531.9	–	531.0	533.0	532.9
	ErQ_3	Er metal [17]	Er_2O_3 [15]	$Er_2(C_2O_4)_3$ [15]	$Er_2(SO_4)_3$ [15]
Er 4d	169.2	167.3	168.6	170.5	169[b]
C 1s	285.7	–	–	290.1	–
O 1s	531.7	–	529.9	532.8	532.8

[a] Divalent.
[b] Estimated. See text for details.

of the oxalates, $RE_2(C_2O_4)_3$, and sulphates, $RE_2(SO_4)_3$ available [15]. The RE 4d binding energies of these materials, and their O and C 1s energies, are compared with those of metallic rare earths [16,17] and the REQ_3s in Table 3. The Er 4d value for $Er_2(SO_4)_3$ in Table 3 is estimated by extrapolation from the data tabulated in [15], since the value of 185.9 eV quoted in that paper is clearly a misprint. Note again the tendency towards higher O 1s binding energies for C–O bonds (the oxalates) compared to C–O–metal bonds. For YbQ_3, the 4d binding energy is much higher than for metallic Yb, since unlike the tabulated compounds, metallic Yb is divalent, not trivalent, as discussed further below. The REQ_3 4d binding energies fall comfortably in the range shown by the other compounds. The range is in any case not particularly large, and in the absence of a larger data set in the literature, the data unfortunately offer little insight into the nature of the RE bonding in the REQ_3 materials.

The spectra in Fig. 7 do not consist of the usual spin-orbit split doublet, but instead are composed of either a single asymmetric peak or a complex multiplet. For lanthanides with unfilled 4f shell, the 4d levels in photoemission spectra form a multiplet due to interaction with that unfilled shell. The 4d photoemission spectra from erbium [17], $4f^{11}$, and its compounds show a complex but unresolved multiplet as shown in Fig. 7. For Yb two cases are possible [18]. Divalent Yb has a full 4f shell, i.e. a $4f^{14}$ configuration, and the 4d spectra show the usual doublet with a 3:2 ratio, while for trivalent Yb, $4f^{13}$, the 4d peaks consist of a multiplet. The transition from doublet to multiplet in the 4d spectra of Yb is illustrated nicely in the oxidation of metallic Yb [19], since metallic Yb is divalent and the sesquioxide is (nominally) trivalent. The multiplet 4d spectrum of YbQ_3 in Fig. 7 is clearly indicative of trivalent Yb. A more direct measure of the 4f occupancy can, however, be obtained from valence band spectra, Fig. 8. At the Mg Kα photon energy, the relative photoelectron cross-sections [9] ensure that the spectra of both YbQ_3 and ErQ_3 in Fig. 8 are completely dominated by the RE 4f signal, with only a shoulder around 5 eV binding energy that could be attributed to ligand orbitals, or possibly the underlying Ag 4d band. Much lower photon energies would be needed, to exploit the relatively

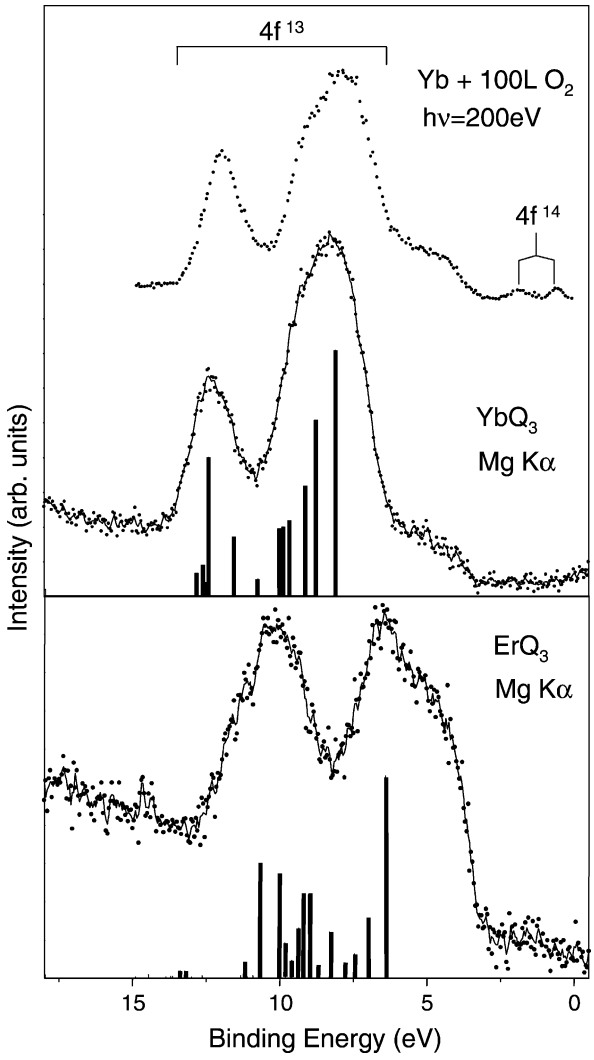

Fig. 8. Comparison of the 4f photoemission spectra of YbQ_3, taken using a photon energy of 1253.6 eV, with that of oxidised Yb metal, from [21], taken using $h\nu = 200$ eV. The $4f^{13}$ multiplet calculation is from [20]. Also shown is the 4f spectrum of ErQ_3 taken using a photon energy of 1253.6 eV.

low cross-section of 4f electrons at low photon energies [9], to render the ligand orbitals visible. The 4f signature of divalent Yb is a spin-orbit split doublet, at a relatively shallow binding energy, with a split of 1.4 eV and an intensity ratio of 4:3. YbQ_3 shows an unresolved multiplet, at binding energies >6 eV, with the two envelopes separated by 5 eV, showing good agreement with Gerken's calculations [20] for the $4f^{13}$ configuration, and with the spectrum of oxidised Yb metal [21]. In comparison, the oxidised Yb data also show an f^{14} doublet, indicating the presence of some divalent Yb, or of mixed valence behaviour in the oxide. The YbQ_3 data show no such doublet, the rising background close to the Fermi level being due to the Mg $K\alpha_2$ satellite line. YbQ_3 would thus appear to be completely trivalent, with no hint of mixed valence behaviour, at least at room temperature.

4. Conclusions

Clean films of REQ_3 can be prepared by evaporation, if suitable degassing is performed, in particular to remove unreacted quinoline. Evaporation begins around 500 K. The mass spectra show features which make evaporation monitoring by mass spectroscopy difficult, notably the high mass of the important fragments and their splitting due to isotope effects. The core level XPS data support the very close similarity of REQ_3 ligands to those of AlQ_3, while the higher O 1s energy observed in REQ_3 is consistent with a more ionic bond than in AlQ_3. The rare earth 4d and 4f data show that, at least at room temperature, Yb in YbQ_3 is entirely trivalent, with no sign of mixed valence behaviour.

Acknowledgements

This work is financially supported by Agilent Technologies and the German Bundesminister für Bildung und Forschung, Project 05 KS1WWA-5. One of us (E. Umbach) acknowledges financial support by the Fond der Chemischen Industrie.

References

[1] C.W. Tang, S.A. Van Slyke, Appl. Phys. Lett. 51 (1987) 913.
[2] J.H. Burroughes, D.D.C. Bradley, A.R. Brown, R.N. Marks, F. Mackay, R.H. Friend, P.L. Burns, A.B. Holmes, Nature (London) 347 (1990) 539.
[3] O.M. Khreis, R.J. Curry, M. Somerton, W.P. Gillin, Org. Electron. 2 (2001) 45.
[4] R.J. Curry, W.P. Gillin, Appl. Phys. Lett. 74 (1999) 798.
[5] R.J. Curry, W.P. Gillin, Appl. Phys. Lett. 75 (1999) 1380.
[6] A. Curioni, M. Boero, W. Andreoni, Chem. Phys. Lett. 294 (1998) 263.
[7] J. Thompson, et al., submitted for publication.
[8] www.webelements.com.
[9] J.J. Yeh, I. Lindau, Atom. Data Nucl. Data Tables 32 (1985) 1.
[10] P.M.A. Sherwood, Practical Surface Analysis, 2nd ed., in: D. Briggs, M. P. Seah (Eds.), Wiley, Chichester, 1990.
[11] S. Kwon, S.C. Kim, Y. Kim, J.-G. Lee, S. Kim, K. Jeong, Appl. Phys. Lett. 79 (2001) 4595.
[12] G. Beamson, D. Briggs, High Resolution XPS of Organic Polymers, Wiley, Chichester, 1992.
[13] R. Treusch, F.J. Himpsel, S. Kakar, L.J. Terminello, C. Heske, T. van Buuren, V.V. Dinh, H.W. Lee, K. Pakbaz, G. Fox, I. Jimenez, J. Appl. Phys. 86 (1999) 88.
[14] A. Curioni, W. Andreoni, R. Treusch, F.J. Himpsel, E. Haskal, P. Seidler, C. Heske, S. Kakar, T. van Buuren, L.J. Terminello, Appl. Phys. Lett. 72 (1998) 1575.
[15] Y. Uwamino, T. Ishizuka, H. Yamatera, J. Electron. Spectrosc. Relat. Phenom. 34 (1984) 67.
[16] S.P. Kowalczyk, N. Edelstein, F.R. McFeely, L. Ley, D.A. Shirley, Chem. Phys. Lett. 29 (1974) 491.
[17] J.F. Moulder, W.F. Stickle, P.E. Sobol, K.D. Bomben, Handbook of X-ray Photoemission Spectroscopy, Physical Electronics, Eden Prairie, 1995.
[18] J.J. Joyce, A.B. Andrews, A.J. Arko, R.J. Bartlett, R.I.R. Blyth, C.G. Olson, P.J. Benning, P.C. Canfield, D.M. Poirier, Phys. Rev. B 54 (1996) 17515.
[19] F.P. Netzer, E. Bertel, Handbook on the Physics and Chemistry of Rare Earths, vol. 5, in: K.A. Gschneidner Jr., L. Eyring (Eds.), North-Holland, Amsterdam, 1982, p. 217.
[20] F. Gerken, J. Phys. Part F: Met. Phys. 13 (1983) 703.
[21] J. Schmidt-May, F. Gerken, R. Nyholm, L.C. Davis, Phys. Rev. B 30 (1984) 5560.